INTERNATIONAL JOURNAL OF
ENERGY AND ENVIRONMENT

Volume 2, Issue 4, 2011 pp.589-604

Journal homepage: www.IJEE.IEEFoundation.org

A CFD analysis on the effect of ambient conditions on the hygro-thermal stresses distribution in a planar ambient air-breathing PEM fuel cell

Maher A.R. Sadiq Al-Baghdadi

Fuel Cell Research Center, International Energy & Environment Foundation, Al-Najaf, P.O.Box 39, Iraq.

Abstract

The need for improved lifetime of air-breathing proton exchange membrane (PEM) fuel cells for portable applications necessitates that the failure mechanisms be clearly understood and life prediction models be developed, so that new designs can be introduced to improve long-term performance. An operating air-breathing PEM fuel cell has varying local conditions of temperature and humidity. As a result of in the changes in temperature and moisture, the membrane, GDL and bipolar plates will all experience expansion and contraction. Because of the different thermal expansion and swelling coefficients between these materials, hygro-thermal stresses are introduced into the unit cell during operation. In addition, the non-uniform current and reactant flow distributions in the cell result in non-uniform temperature and moisture content of the cell which could in turn, potentially causing localized increases in the stress magnitudes, and this leads to mechanical damage, which can appear as through-the-thickness flaws or pinholes in the membrane, or delaminating between the polymer membrane and gas diffusion layers. Therefore, in order to acquire a complete understanding of these damage mechanisms in the membranes and gas diffusion layers, mechanical response under steady-state hygro-thermal stresses should be studied under real cell operation conditions.

A three-dimensional, multi–phase, non-isothermal computational fluid dynamics model of a planar ambient air-breathing, proton exchange membrane fuel cell has been developed and used to study the effects of ambient conditions on the temperature distribution, displacement, deformation, and stresses inside the cell. The behaviour of the fuel cell during operation has been studied and investigated under real cell operating conditions. A unique feature of the present model is to incorporate the effect of mechanical, hygro and thermal stresses into actual three-dimensional fuel cell model. The results show that the non-uniform distribution of stresses, caused by the temperature gradient in the cell, induces localized bending stresses, which can contribute to delaminating between the membrane and the gas diffusion layers. The non-uniform distribution of stresses can also contribute to delaminating between the gas diffusion layers and the current collectors. These stresses may explain the occurrence of cracks and pinholes in the fuel cells components under steady–state loading during regular cell operation, especially in the high loading conditions. The results showed that the ambient conditions (ambient temperature and relative humidity) have a strong impact on the temperature distribution and hygro-thermal stresses inside the cell.

Keywords: Air-breathing PEM fuel cell; Ambient conditions; CFD; Hygro-Thermal stresses; Nafion.

1. Introduction

Fuel cell system is an advanced power system for the future that is sustainable, clean and environmental friendly. Small fuel cells have provided significant advantages in portable electronic applications over conventional battery systems. Competitive costs, instant recharge, and high energy density make fuel cells ideal for supplanting batteries in portable electronic devices. However, the typical PEM fuel cell system with its heavy reliance on subsystems for cooling, humidification and air supply would not be practical in small applications. The air-breathing PEM fuel cells without moving parts (external humidification instrument, fans or pumps) are one of the most competitive candidates for future portable-power applications. In air-breathing PEM fuel cell, the cathode side of the cell is directly open to ambient air. The oxygen needed by the fuel cell electrochemical reaction is taken directly from the surrounding air by natural convection and diffusion through the gas diffusion backing into the cathode electrode. For portable applications like laptops, camcorders, and mobile phones the requirements of the fuel cell systems are even more specific than for stationary and vehicular applications. The requirements for portable applications are mostly focused on lifetime, size and weight of the system as well as the temperature.

Ambient conditions such as temperature and relative humidity of surroundings played an important role on the air-breathing fuel cell performance, because membrane hydration, water removal and oxygen transport at the cathode were influenced by the ambient temperature and humidity [1]. Proper water management requires meeting two conflicting needs: adequate membrane hydration and avoidance of water flooding in the cathode catalyst layer and/or gas diffusion layer [2]. Water management is related with air supply to the cathode and is one of the crucial factors in an air-breathing PEM fuel cell system, due the lack of control of ambient air stream conditions (flow stoichiometry, temperature, and humidity).

In order to retain the optimum hydration level of the air-breathing PEM fuel cell, water produced at the cathode has to be supplied to the membrane and the anode. However, too much water may lead to cathode flooding, which limits the access of oxygen to the active surface of the catalyst particles. Under certain ambient and operating conditions, such as low humidity, high temperatures, and low current densities, dehumidification of the membrane may occur, resulting in deterioration of protonic conductivity, increasing resistive losses, and increasing MEA temperature. In the extreme case of complete drying, local burnout of the membrane may result [3]. Thus, proper hydration of the membrane electrode assembly (MEA) and removal of water from cathode through water management is critical to maintain membrane conductivity and performance. Thermal management is also required to remove the heat produced by the electrochemical reaction in order to prevent drying out of the membrane, which in turn can result not only in reduced performance but also in eventual rupture of the membrane. Thermal management is also essential for the control of the water evaporation or condensation rates [1-3].

The need for improved lifetime of air-breathing proton exchange membrane (PEM) fuel cells necessitates that the failure mechanisms be clearly understood and life prediction models be developed, so that new materials can be introduced to improve long-term performance. An operating air-breathing PEM fuel cell has varying local conditions of temperature and humidity. As a result of in the changes in temperature and moisture, the membrane, GDL and bipolar plates will all experience expansion and contraction. Because of the different thermal expansion and swelling coefficients between these materials, hygro-thermal stresses are introduced into the unit cell during operation [4, 5]. In addition, the non-uniform current and reactant flow distributions in the cell result in non-uniform temperature and moisture content of the cell which could in turn, potentially causing localized increases in the stress magnitudes, and this leads to mechanical damage, which can appear as through-the-thickness flaws or pinholes in the membrane, or delaminating between the polymer membrane and gas diffusion layers [6-10]. Therefore, in order to acquire a complete understanding of these damage mechanisms in the membrane electrode assembly (MEA), mechanical response under steady-state hygro-thermal stresses should be studied under real cell operation conditions [11, 12].

The development of physically representative models that allow reliable simulation of the processes under realistic conditions is essential to the development and optimization of fuel cells, improve long-term performance, the introduction of cheaper materials and fabrication techniques, and the design and development of novel architectures. The difficult experimental environment of fuel cell systems has stimulated efforts to develop models that could simulate and predict multi-dimensional coupled transport of reactants, heat and charged species using computational fluid dynamic (CFD) methods. The strength of the CFD numerical approach is in providing detailed insight into the various transport mechanisms and their interaction, and in the possibility of performing parameters sensitivity analyses.

ISSN 2076-2895 (Print), ISSN 2076-2909 (Online)

In this work, a three-dimensional, multi-phase, CFD model of a planar air-breathing PEM fuel cell has been developed and used to investigate the effects of ambient conditions (ambient temperature and relative humidity) on the temperature distribution, displacement, deformation, and stresses inside the cell.

2. Model description

The present work presents a comprehensive three–dimensional, multi–phase, non-isothermal model of a planar ambient air-breathing PEM fuel cell that incorporates the significant physical processes and the key parameters affecting fuel cell performance. The following assumptions are made: *(i.)* to alleviate the need for air distribution channels, along with the necessary pumps and fans, the cathode gas diffusion layer is in direct contact with the ambient air; *(ii.)* the ionic conductivity of the membrane is constant; *(iii.)* the membrane is impermeable to gases and cross-over of reactant gases is neglected; *(iv.)* the gas diffusion layer is homogeneous and isotropic; *(v.)* the flow in the natural convection region is laminar; *(vi.)* the produced water is in the vapour phase; *(vii.)* two-phase flow inside the porous media; *(viii.)* both phases occupy a certain local volume fraction inside the porous media and their interaction is accounted for through a multi-fluid approach; *(ix.)* external humidification systems are eliminated and the fuel cell relies on the ambient relative humidity and water production in the cathode for the humidification of the membrane; *(x.)* the circulating ambient air facilitates the cooling of the fuel cell in lieu of a dedicated heat management system.

The model accounts for both gas and liquid phase in the same computational domain, and thus allows for the implementation of phase change inside the gas diffusion layers. The model includes the transport of gaseous species, liquid water, protons, energy, and water dissolved in the ion-conducting polymer. Water transport inside the porous gas diffusion layer and catalyst layer is described by two physical mechanisms: viscous drag and capillary pressure forces, and is described by advection within the gas channel. Water transport across the membrane is also described by two physical mechanisms: electro-osmotic drag and diffusion. Water is assumed to be exchanged among three phases; liquid, vapour, and dissolved, and equilibrium among these phases is assumed.

In addition to the new and complex geometry, a unique feature of the present model is to incorporate the effect of hygro and thermal stresses into actual three-dimensional fuel cell model. This model also takes into account convection and diffusion of different species in the channel as well as in the porous gas diffusion layer, heat transfer in the solids as well as in the gases, and electrochemical reactions. The model reflects the influence of numerous parameters on fuel cell performance including geometry, materials, operating and others to investigate the in situ stresses in polymer membranes. The present multi-phase model is capable of identifying important parameters for the wetting behaviour of the gas diffusion layers and can be used to identify conditions that might lead to the onset of pore plugging, which has a detrimental effect of the fuel cell performance.

2.1 Computational domain

The full computational domains for the planar air-breathing PEM fuel cell consists of anode gas flow field and the membrane electrode assembly is shown in Figure (1a). A schematic description of a planer air-breathing PEM fuel cell stack is also shown in Figure (1b). The cathode side of the cell is directly open to ambient air. The oxygen needed by the fuel cell reaction is transferred by natural convection and diffusion through the gas diffusion backing into the cathode electrode. The perforated current collector plate on the cathode side is used in order to ensure good mechanical, thermal, and electrical contact between the central parts of the gas diffusion backing and Membrane-Electrode-Assembly (MEA).

2.2 Model equations

2.2.1 Air and fuel gas flow

In natural convection region, the transport equations solved in the ambient air include continuity, momentum, energy and mass transport equations. In the fuel channel, the gas-flow field is obtained by solving the steady-state Navier-Stokes equations, i.e. the continuity equation, the mass conservation equation for each phase yields the volume fraction (r) and along with the momentum equations the pressure distribution inside the channel. The continuity equation for the gas phase inside the channel is given by;

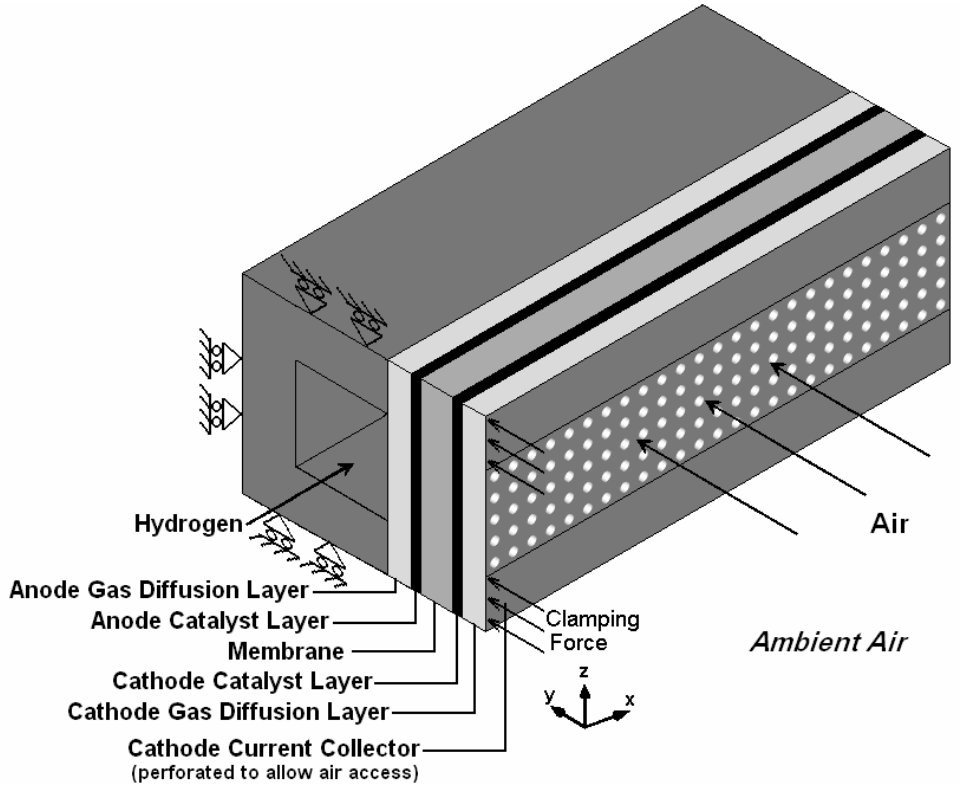

(a)

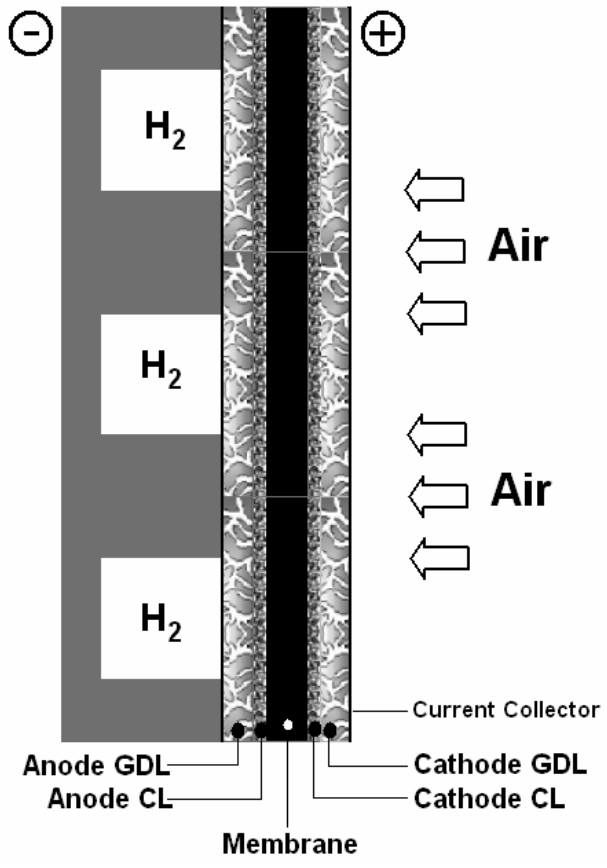

(b)

Figure 1. (a) Three-dimensional computational domain of a planar ambient air-breathing PEM fuel cell and (b) longitudinal cross section of 3-cell fuel cell stack

$$\nabla \cdot \left(r_g \rho_g \mathbf{u}_g \right) = 0 \tag{1}$$

and for the liquid phase inside the channel becomes;

$$\nabla \cdot \left(r_l \rho_l \mathbf{u}_l \right) = 0 \tag{2}$$

where $\boldsymbol{u}$ is velocity vector (m/s), ρ is density (kg/m^3). Subscript (g) is a gas phase and (l) is a liquid phase.

Two sets of momentum equations are solved in the channel, and they share the same pressure field. Under these conditions, it can be shown that the momentum equations becomes;

$$\nabla \cdot \left(\rho_g \mathbf{u}_g \otimes \mathbf{u}_g - \mu_g \nabla \mathbf{u}_g \right) = -\nabla r_g \left(P + \frac{2}{3} \mu_g \nabla \cdot \mathbf{u}_g \right) + \nabla \cdot \left[\mu_g \left(\nabla \mathbf{u}_g \right)^T \right] \tag{3}$$

$$\nabla \cdot \left(\rho_l \mathbf{u}_l \otimes \mathbf{u}_l - \mu_l \nabla \mathbf{u}_l \right) = -\nabla r_l \left(P + \frac{2}{3} \mu_l \nabla \cdot \mathbf{u}_l \right) + \nabla \cdot \left[\mu_l \left(\nabla \mathbf{u}_l \right)^T \right] \tag{4}$$

where P is pressure (Pa), μ is viscosity [kg/(m·s)].

The mass balance is described by the divergence of the mass flux through diffusion and convection. Multiple species are considered in the gas phase only, and the species conservation equation in multi-component, multi-phase flow can be written in the following expression for species i;

$$\nabla \cdot \left[- r_g \rho_g y_i \sum_{j=1}^{N} D_{ij} \frac{M}{M_j} \left[\left(\nabla y_j + y_j \frac{\nabla M}{M} \right) + \left(x_j - y_j \right) \frac{\nabla P}{P} \right] + r_g \rho_g y_i \cdot \mathbf{u}_g + D_i^T \frac{\nabla T}{T} \right] = 0 \tag{5}$$

where T is temperature (K), y is mass fraction, x is mole fraction. Subscript i denotes oxygen at the cathode side and hydrogen at the anode side, and j is water vapour in both cases. Nitrogen is the third species at the cathode side.

The Maxwell-Stefan diffusion coefficients of any two species are dependent on temperature and pressure. They can be calculated according to the empirical relation based on kinetic gas theory [13];

$$D_{ij} = \frac{T^{1.75} \times 10^{-3}}{P \left[\left(\sum_k V_{ki} \right)^{1/3} + \left(\sum_k V_{kj} \right)^{1/3} \right]^2} \left[\frac{1}{M_i} + \frac{1}{M_j} \right]^{1/2} \tag{6}$$

In this equation, pressure is in [atm] and the binary diffusion coefficient is in [cm^2/s]. The values for $\left(\sum V_{ki} \right)$ are given by Fuller et al. [13].

The temperature field is obtained by solving the convective energy equation;

$$\nabla \cdot \left(r_g \left(\rho_g C p_g \mathbf{u}_g T - k_g \nabla T \right) \right) = 0 \tag{7}$$

where Cp_g is a specific heat capacity (J/(kg.K)), and k_g is gases thermal conductivity (W/(m.K)).

The gas phase and the liquid phase are assumed to be in thermodynamic equilibrium; hence the temperature of the liquid water is the same as the gas phase temperature.

2.2.2 Gas diffusion layers

The physics of multiple phases through a porous medium is further complicated here with phase change and the sources and sinks associated with the electrochemical reaction. The equations used to describe transport in the gas diffusion layers are given below. Mass transfer in the form of evaporation ($\dot{m}_{phase} > 0$) and condensation ($\dot{m}_{phase} < 0$) is assumed. Where $\dot{m}_{phase}$ is mass transfer: for evaporation ($\dot{m}_{phase} = \dot{m}_{evap}$) and for condensation ($\dot{m}_{phase} = \dot{m}_{cond}$) (kg/s).

So that the mass balance equations for both phases are;

$$\nabla \cdot \left((1 - sat) \rho_g \varepsilon \mathbf{u}_g \right) = \dot{m}_{phase} \tag{8}$$

$$\nabla \cdot \left(sat . \rho_l \varepsilon \mathbf{u}_l \right) = \dot{m}_{phase} \tag{9}$$

where *sat* is saturation, ε is porosity.

The momentum equation for the gas phase reduces to Darcy's law, which is, however, based on the relative permeability for the gas phase (KP). The relative permeability accounts for the reduction in pore space available for one phase due to the existence of the second phase [14, 15].
The momentum equation for the gas phase inside the gas diffusion layer becomes;

$$\mathbf{u}_g = -(1-sat)\frac{Kp}{\mu_g}\nabla P \tag{10}$$

where Kp is hydraulic permeability (m^2).

Two liquid water transport mechanisms are considered; shear, which drags the liquid phase along with the gas phase in the direction of the pressure gradient, and capillary forces, which drive liquid water from high to low saturation regions [14, 15]. Therefore, the momentum equation for the liquid phase inside the gas diffusion layer becomes;

$$\mathbf{u}_l = -\frac{KP_l}{\mu_l}\nabla P + \frac{KP_l}{\mu_l}\frac{\partial P_c}{\partial sat}\nabla sat \tag{11}$$

where P_c is capillary pressure (Pa).

The functional variation of capillary pressure with saturation is calculated as follows [15];

$$P_c = \sigma\left(\frac{\varepsilon}{KP}\right)^{1/2}\left(1.417(1-sat) - 2.12(1-sat)^2 + 1.263(1-sat)^3\right) \tag{12}$$

where σ is surface tension (N/m).

The liquid phase consists of pure water, while the gas phase has multi components. The transport of each species in the gas phase is governed by a general convection-diffusion equation in conjunction which the Stefan-Maxwell equations to account for multi species diffusion;

$$\nabla\cdot\left[\begin{array}{c} -(1-sat)\rho_g\varepsilon y_i\sum_{j=1}^{N}D_{ij}\frac{M}{M_j}\left[\left(\nabla y_j + y_j\frac{\nabla M}{M}\right)+\left(x_j-y_j\right)\frac{\nabla P}{P}\right]+ \\ (1-sat)\rho_g\varepsilon y_i\cdot\mathbf{u}_g + \varepsilon D_i^T\frac{\nabla T}{T}\end{array}\right] = \dot{m}_{phase} \tag{13}$$

In order to account for geometric constraints of the porous media, the diffusivities are corrected using the Bruggemann correction formula [16];

$$D_{ij}^{eff} = D_{ij}\times\varepsilon^{1.5} \tag{14}$$

The heat transfer in the gas diffusion layers is governed by the energy equation as follows;

$$\nabla\cdot\left((1-sat)\left(\rho_g\varepsilon Cp_g\mathbf{u}_g T - k_{eff,g}\varepsilon\nabla T\right)\right) = \varepsilon\beta\left(T_{solid}-T\right) - \varepsilon\dot{m}_{phase}\Delta H_{evap} \tag{15}$$

where k_{eff} is effective electrode thermal conductivity (W/m·K), the term ($\varepsilon\beta\left(T_{solid}-T\right)$), on the right hand side, accounts for the heat exchange to and from the solid matrix of the GDL. β is a modified heat transfer coefficient that accounts for the convective heat transfer in [W/m^2] and the specific surface area [m^2/m^3] of the porous medium [17]. Hence, the unit of β is [W/m^3]. The gas phase and the liquid phase are assumed to be in thermodynamic equilibrium, i.e., the liquid water and the gas phase are at the same temperature.

The potential distribution in the gas diffusion layers is governed by;

$$\nabla\cdot\left(\lambda_e\nabla\phi\right) = 0 \tag{16}$$

where λ_e is electrode electronic conductivity (S/m).

In order to account for the magnitude of phase change inside the GDL, expressions are required to relate the level of over- and undersaturation as well as the amount of liquid water present to the amount of water undergoing phase change. In the present work, the procedure of Berning and Djilali [15] was used to account for the magnitude of phase change inside the GDL.

2.2.3 Catalyst layers

The catalyst layer is treated as a thin interface, where sink and source terms for the reactants are implemented. Due to the infinitesimal thickness, the source terms are actually implemented in the last grid cell of the porous medium. At the cathode side, the sink term for oxygen is given by [18, 19];

$$S_{O_2} = -\frac{M_{O_2}}{4F} i_c \tag{17}$$

where M is molecular weight (kg/mole), F is Faraday's constant = 96487 (C/mole), i is local current density (A/m^2).

Whereas the sink term for hydrogen is specified as;

$$S_{H_2} = -\frac{M_{H_2}}{2F} i_a \tag{18}$$

The production of water is modelled as a source terms, and hence can be written as;

$$S_{H_2O} = \frac{M_{H_2O}}{2F} i_c \tag{19}$$

The generation of heat in the cell is due to entropy changes as well as irreversibilities due to the activation overpotential [20];

$$\dot{q} = \left[\frac{T(-\Delta s)}{n_e F} + \eta_{act} \right] i \tag{20}$$

where η_{act} is activation over potential (V), n_e is number of electrons transfer, ΔS is entropy change of cathode side reaction.

The local current density distribution in the catalyst layers is modelled by the Butler-Volmer equation [21, 22];

$$i_c = i_{o,c}^{ref} \left(\frac{C_{O_2}}{C_{O_2}^{ref}} \right) \left[\exp\left(\frac{\alpha_a F}{RT} \eta_{act,c} \right) + \exp\left(-\frac{\alpha_c F}{RT} \eta_{act,c} \right) \right] \tag{21}$$

$$i_a = i_{o,a}^{ref} \left(\frac{C_{H_2}}{C_{H_2}^{ref}} \right)^{1/2} \left[\exp\left(\frac{\alpha_a F}{RT} \eta_{act,a} \right) + \exp\left(-\frac{\alpha_c F}{RT} \eta_{act,a} \right) \right] \tag{22}$$

where $C_{\mathrm{H_2}}$ is local hydrogen concentration (mole/m^3), $C_{\mathrm{H_2}}^{\mathrm{ref}}$ is reference hydrogen concentration (mole/m^3), $C_{\mathrm{O_2}}$ is local oxygen concentration (mole/m^3), $C_{\mathrm{O_2}}^{\mathrm{ref}}$ is reference oxygen concentration (mole/m^3), C_{p} is specific heat capacity [J/(kg·K)], D is diffusion coefficient (m^2/s), $i_{\mathrm{o,a}}^{\mathrm{ref}}$ is anode reference exchange current density, $i_{\mathrm{o,c}}^{\mathrm{ref}}$ is cathode reference exchange current density, R is universal gas constant (=8.314 J/(mole·K)), s is specific entropy [J/(mole·K)], α_{a} is charge transfer coefficient, anode side, and α_{c} is charge transfer coefficient, cathode side.

2.2.4 Membrane

The balance between the electro-osmotic drag of water from anode to cathode and back diffusion from cathode to anode yields the net water flux through the membrane [23];

$$N_W = n_d M_{H_2O} \frac{i}{F} - \nabla \cdot (\rho D_W \nabla c_W) \tag{23}$$

where N_{w} is net water flux across the membrane (kg/m^2·s), n_{d} is electro-osmotic drag coefficient.
The water diffusivity in the polymer can be calculated as follow [24];

$$D_W = 1.3 \times 10^{-10} \exp\left[2416 \left(\frac{1}{303} - \frac{1}{T} \right) \right] \tag{24}$$

The variable c_W represents the number of water molecules per sulfonic acid group (i.e. $\mathrm{mol}\, H_2O / \mathrm{equivalent}\, SO_3^{-1}$).The water content in the electrolyte phase is related to water vapour activity via [25, 26];

$$c_W = 0.043 + 17.81a - 39.85a^2 + 36.0a^3 \quad (0 < a \le 1)$$
$$c_W = 14.0 + 1.4(a-1) \quad (1 < a \le 3) \tag{25}$$
$$c_W = 16.8 \quad (a \ge 3)$$

The water vapour activity given by;

$$a = \frac{x_W P}{P_{sat}} \tag{26}$$

Heat transfer in the membrane is governed by [27];

$$\nabla \cdot (k_{mem} \cdot \nabla T) = 0 \tag{27}$$

where k_{mem} is membrane thermal conductivity [W/(m·K)].

The potential loss in the membrane is due to resistance to proton transport across membrane, and is governed by;

$$\nabla \cdot (\lambda_m \nabla \phi) = 0 \tag{28}$$

where λ_{m} is membrane ionic conductivity (S/m).

2.2.5 Stresses in fuel cell components

Assuming linear response within the elastic region, the isotropic Hooke's law is used to determine the stress tensor.

$$\Omega = \mathbf{G}.\pi \tag{29}$$

where **G** is the constitutive matrix, π is the strain.

Using hygrothermoelasticity theory, the effects of temperature and moisture as well as the mechanical forces on the behaviour of elastic bodies have been addressed. In the present work, the total strain tensor is determined using the same expression of Kusoglu et al. [12];

$$\pi = \pi^M + \pi^T + \pi^S \tag{30}$$

where, π^M is the contribution from the mechanical forces and π^T, π^S are the thermal and swelling induced strains, respectively.

The thermal strains resulting from a change in temperature of an unconstrained isotropic volume are given by;

$$\pi^T = \wp(T - T_{\text{Re}\,f}) \tag{31}$$

where $\wp$ is thermal expansion (1/K).

Similarly, the swelling strains caused by moisture uptake are given by;

$$\pi^S = \text{ƛ}_{mem}(\Re - \Re_{\text{Re}\,f}) \tag{32}$$

where ƛ_{mem} is the membrane humidity swelling-expansion tensor (1/%), $\Re$ is the relative humidity (%).

Following the work [12], the swelling-expansion for the membrane, ƛ_{mem}, is expressed as a polynomial function of humidity and temperature as follows;

$$\text{ƛ}_{mem} = \sum_{i,j=1}^{4} C_{ij} T^{4-i} \Re^{4-j} \tag{33}$$

where C_{ij} is the polynomial constants, see Ref. [12].

The geometric and the base case operating conditions are listed in Table 1. Values of the electrochemical transport parameters for the base case operating conditions are listed in Table 2. The material properties for the fuel cell components used in this model are taken from reference [12] and are shown in Tables 3-5. The initial conditions corresponding to zero stress-state are defined; all components of the cell stack are set to reference temperature 20 C, and relative humidity 35% (corresponding to the assembly conditions) [11, 12, 28]. In addition, a constant pressure of (1 MPa) is applied on the upper surface of cathode, corresponding to a case where the fuel cell is equipped with the o-ring cathode current collectors to control the clamping force.

Table 1. Geometrical and operational parameters for base case conditions

Parameter	***Sym.***	**Value**	**Unit**
Channel length	L	0.05	m
Channel width	W	1e-3	m
Channel height	H	1e-3	m
Land area width	W_{land}	1e-3	m
Gas diffusion layer thickness	δ_{GDL}	0.26e-3	m
Wet membrane thickness (Nafion® 117)	δ_{mem}	0.23e-3	m
Catalyst layer thickness	δ_{CL}	0.0287e-3	m
Hydrogen reference mole fraction	$x_{H_2}^{ref}$	0.84639	-
Oxygen reference mole fraction	$x_{O_2}^{ref}$	0.17774	-
Anode pressure	P_a	1	atm
Cathode pressure	P_c	1	atm

Table 2. Electrode and membrane parameters for base case operating conditions

Parameter	**Sym.**	**Value**	**Unit**	**Ref.**
Electrode porosity	ε	0.4	-	[18]
Electrode electronic conductivity	λ_e	100	S/m	[27]
Membrane ionic conductivity	λ_m	17.1223	S/m	[18]
Transfer coefficient, anode side	α_a	0.5	-	[19]
Transfer coefficient, cathode side	α_c	1	-	[22]
Cathode ref. exchange current density	$i_{o,c}^{ref}$	1.8081e-3	A/m^2	[14]
Anode ref. exchange current density	$i_{o,a}^{ref}$	2465.598	A/m^2	[14]
Electrode thermal conductivity	k_{eff}	1.3	$W/m.K$	[16]
Membrane thermal conductivity	k_{mem}	0.455	$W/m.K$	[16]
Electrode hydraulic permeability	kp	1.76e-11	m^2	[21]
Entropy change of cathode side reaction	ΔS	-326.36	$J/mole.K$	[20]
Heat transfer coefficient between solid & gas phase	β	4e6	W/m^3	[17]
Protonic diffusion coefficient	D_{H^+}	4.5e-9	m^2/s	[18]
Fixed-charge concentration	c_f	1200	$mole/m^3$	[18]
Fixed-site charge	z_f	-1	-	[18]
Electro-osmotic drag coefficient	n_d	2.5	-	[23]
Droplet diameter	D_{drop}	1.0×10^{-8}	m	[15]
Condensation constant	C	1.0×10^{-5}	-	[15]
Scaling parameter for evaporation	ϖ	0.01	-	[15]

Table 3. Material properties used in the model

Parameter	Symbol	Value	Unit
Electrode Poisson's ratio	$\Im_{GDL}$	0.25	-
Membrane Poisson's ratio	$\Im_{mem}$	0.25	-
Electrode thermal expansion	α_{GDL}	-0.8e-6	$1/K$
Membrane thermal expansion	α_{mem}	123e-6	$1/K$
Electrode Young's modulus	Ψ_{GDL}	1e10	Pa
Membrane Young's modulus	Ψ_{mem}	Table 4	Pa
Electrode density	ρ_{GDL}	400	kg/m^3
Membrane density	ρ_{mem}	2000	kg/m^3
Membrane humidity swelling-expansion tensor	$\hat{\lambda}_{mem}$	from eq.(33)	$1/\%$

Table 4. Young's modulus at various temperatures and humidities of Nafion

Young's modulus [MPa]	**Relative humidity [%]**			
	30	**50**	**70**	**90**
T=25 C	197	192	132	121
T=45 C	161	137	103	70
T=65 C	148	117	92	63
T=85 C	121	85	59	46

Table 5. Yield strength at various temperatures and humidities of Nafion

Yield stress [MPa]	**Relative humidity [%]**			
	30	**50**	**70**	**90**
T=25 C	6.60	6.14	5.59	4.14
T=45 C	6.51	5.21	4.58	3.44
T=65 C	5.65	5.00	4.16	3.07
T=85 C	4.20	3.32	2.97	2.29

3. Results and discussion

The governing equations were discretized using a finite volume method and solved using a multi-physics computational fluid dynamics code. Stringent numerical tests were performed to ensure that the solutions were independent of the grid size. A computational quadratic finer mesh consisting of a total of 92305 nodes and 501867 meshes ware found to provide sufficient spatial resolution (Figure 2). The coupled set of equations was solved iteratively, and the solution was considered to be convergent when the relative error in each field between two consecutive iterations was less than 1.0×10^{-6}. The calculations presented here have all been obtained on a Pentium IV PC (3 GHz, 3GB RAM) using Windows XP operating system. Results for the cell operate at nominal current density of 0.4 A/cm^2 is discussed in this section.

The ambient conditions have a strong impact on the fuel cell performance. Ambient temperature and relative humidity impacted all three major electrochemical loss components of the air-breathing fuel cell: activation, resistive, and mass transfer. Activation losses were typically the largest loss component. However, these were affected weakly by varying ambient conditions. A small increase in activation losses was showed at high ambient temperature and low humidity conditions (probably due to catalyst dry-out). Resistive losses were most strongly affected by ambient conditions and dominated fuel cell losses during dry-out. The membrane resistance decreases due to membrane self-humidification with

product water and self-heating with reaction heat, and membrane resistance increases due to excessive evaporation from the cathode surface. Mass transfer losses typically became important at high current density. Furthermore, low ambient temperatures, and high ambient humidity both tended to increase mass transfer losses due to flooding of the GDL.

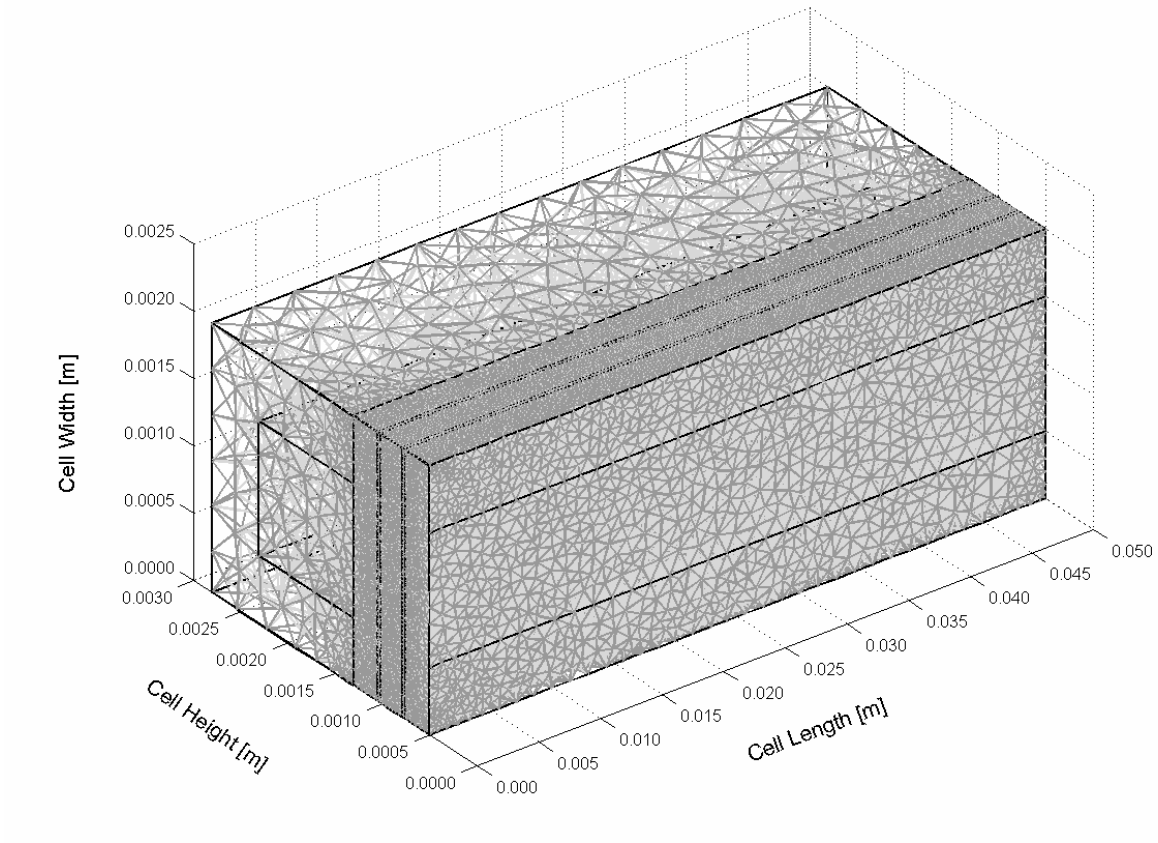

Figure 2. Computational mesh of an ambient air-breathing PEM fuel cell (quadratic)

The temperature distribution in the air-breathing fuel cell is dependent on the membrane electrode assembly water content. The net water balance of the cell is a complex coupling of cell self-heating and water production as well as the convection of heat and water vapour to the environment. The temperature distribution inside the cell can be shown in Figures 3 and 4 for two cases of the ambient relative humidity values. In both cases, the highest temperatures are located at the cathode catalyst layer, implying that major heat generation takes place in this region. The minimum temperature with lower gradient appears in the cell of the higher ambient relative humidity case (Figure 3). The temperature difference between the cathode catalyst layer and ambient air temperature is about 5 K. Further, the temperature profiles are more uniform compared with the result of the lower ambient relative humidity case (Figure 4). This behaviour is consistent with a more hydrated membrane, lower ohmic losses, and reduced joule heating.
Thermal management is required to remove the heat produced by the electrochemical reaction in order to prevent drying out of the membrane and excessive thermal stresses that result in rupture of the membrane. The small temperature differential between the fuel cell stack and the operating environment make thermal management a challenging problem in PEM fuel cells. As the ambient temperature increases, the air-breathing fuel cell rejects less heat and the GDL temperature increases (Figure 5). At high temperature and low relative humidity the membrane dries out due to evaporation of product water from the open cathode surface, and the cell potential drops. At low temperature and high relative humidity the cell floods at high current density.
In conclusion, the self-heating and self-humidifying effects of passive fuel cells are balanced by the transfer of heat and water to the ambient. Optimal performance of air-breathing cells is therefore a complex function of ambient and load conditions as well as the cell design.

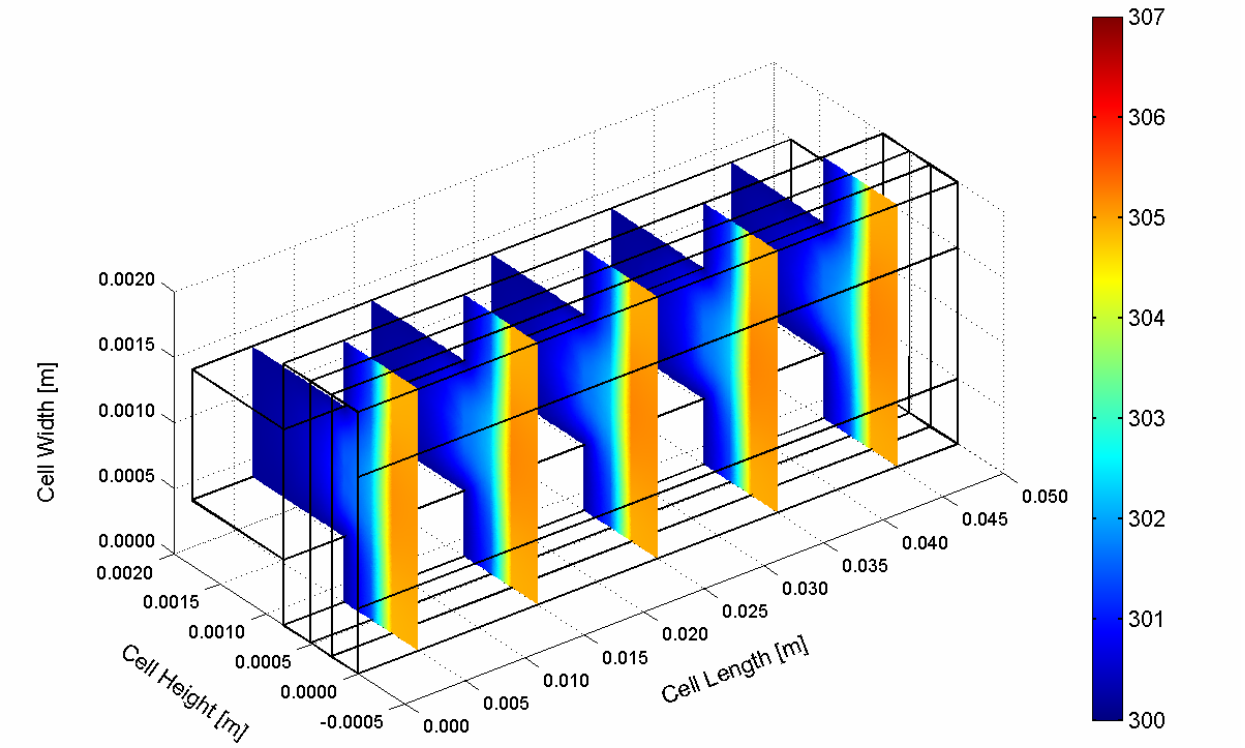

Figure 3. Temperature distribution inside the cell at ambient temperature of 300.15 K (27 C) and relative humidity of 80%.

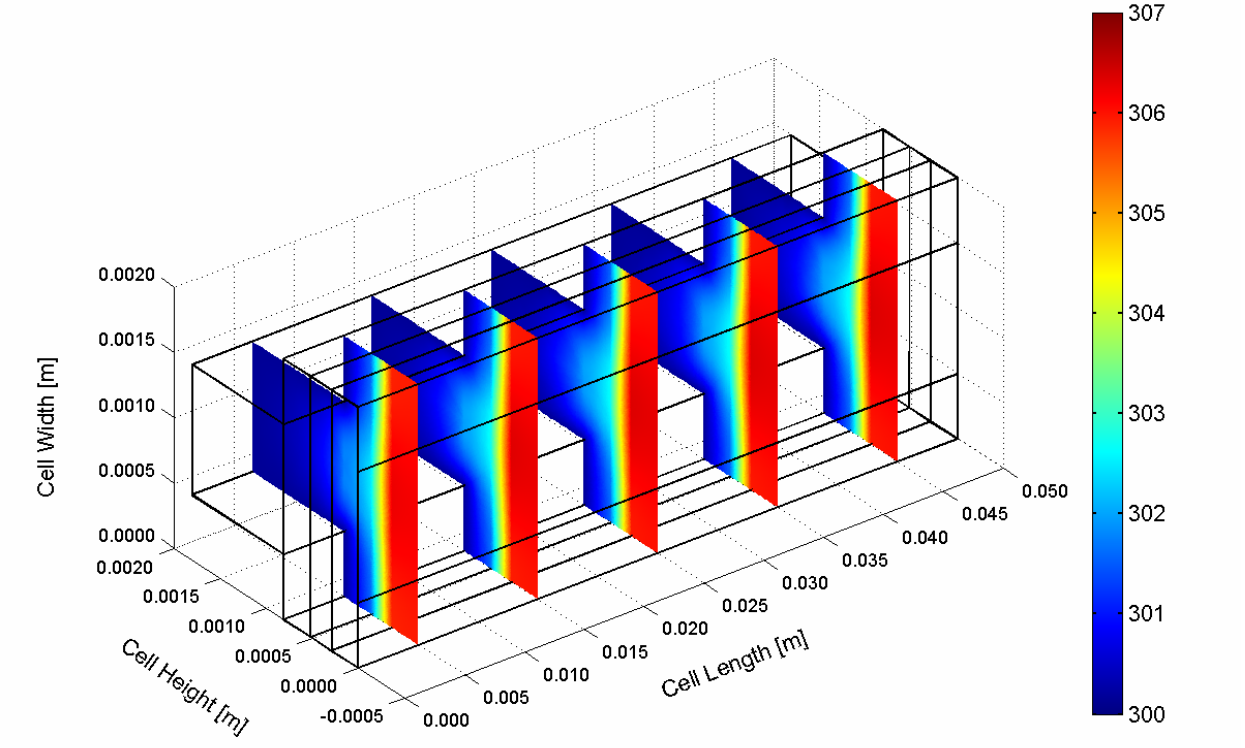

Figure 4. Temperature distribution inside the cell at ambient temperature of 300.15 K (27 C) and relative humidity of 20%.

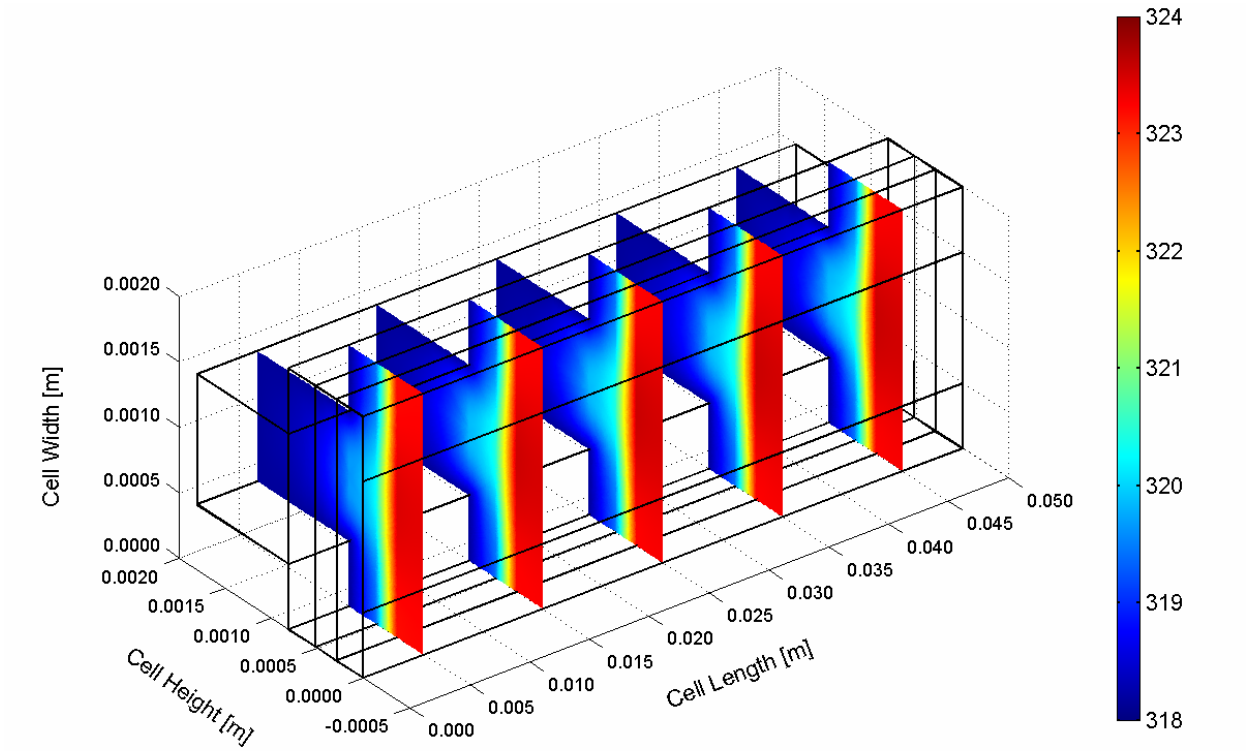

Figure 5. Temperature distribution inside the cell at ambient temperature of 318.15 K (45 C) and relative humidity of 80%.

The durability of proton exchange membranes used in fuel cells is a major factor in the operating lifetime of fuel cell systems. The stresses distribution in the air-breathing fuel cells is affected by ambient conditions (ambient temperature and relative humidity). The stresses distribution (in MPa) in Membrane-Electrode-Assembly (MEA) that developed during the cell operating can be seen in Figures (6-8), for different ambient conditions. The figures show von Mises stress distribution (contour plots) and deformation shape (scale enlarged 200 times) for MEA. Because of the different thermal expansion and swelling coefficients between gas diffusion layers and membrane materials with non-uniform temperature distributions in the cell during operation, hygro-thermal stresses and deformation are introduced. The non-uniform distribution of stress, caused by the temperature gradient in the MEA, induces localized bending stresses, which can contribute to delaminating between the membrane and the GDLs. It can be seen that the maximum deformation and stress occurs, where the temperature is highest, which is near the cathode side area. The maximum stress appears in the cathode side surface of the membrane, implying that major heat generation takes place near this region. It can be seen also that the total displacement and the degree of the deformation in membrane are directly related to the increasing of ambient temperature and decreasing of relative humidity, due to increasing of heat generation.

4. Conclusions

A full three-dimensional computational fluid dynamics model of a planar air-breathing PEM fuel cell has been developed and used to investigate the cell at varying ambient temperature and relative humidity. Detailed analyses of the temperature distribution and the hygro and thermal stresses inside the cell under various ambient conditions have been conducted and examined. The analysis helped identifying critical parameters and shed insight into the physical mechanisms leading to a fuel cell performance and durability under various ambient conditions. The model is shown to be able to: (1) understand the many interacting, complex electrochemical and transport phenomena that cannot be studied experimentally; (2) identify limiting steps and components; and (3) provide a computer-aided tool for the design and optimization of future fuel cells to improve their lifetime with a much higher power density and lower cost. The analysis offers valuable physical insight towards design of a cell and a cell stack, to be considered in a future study.

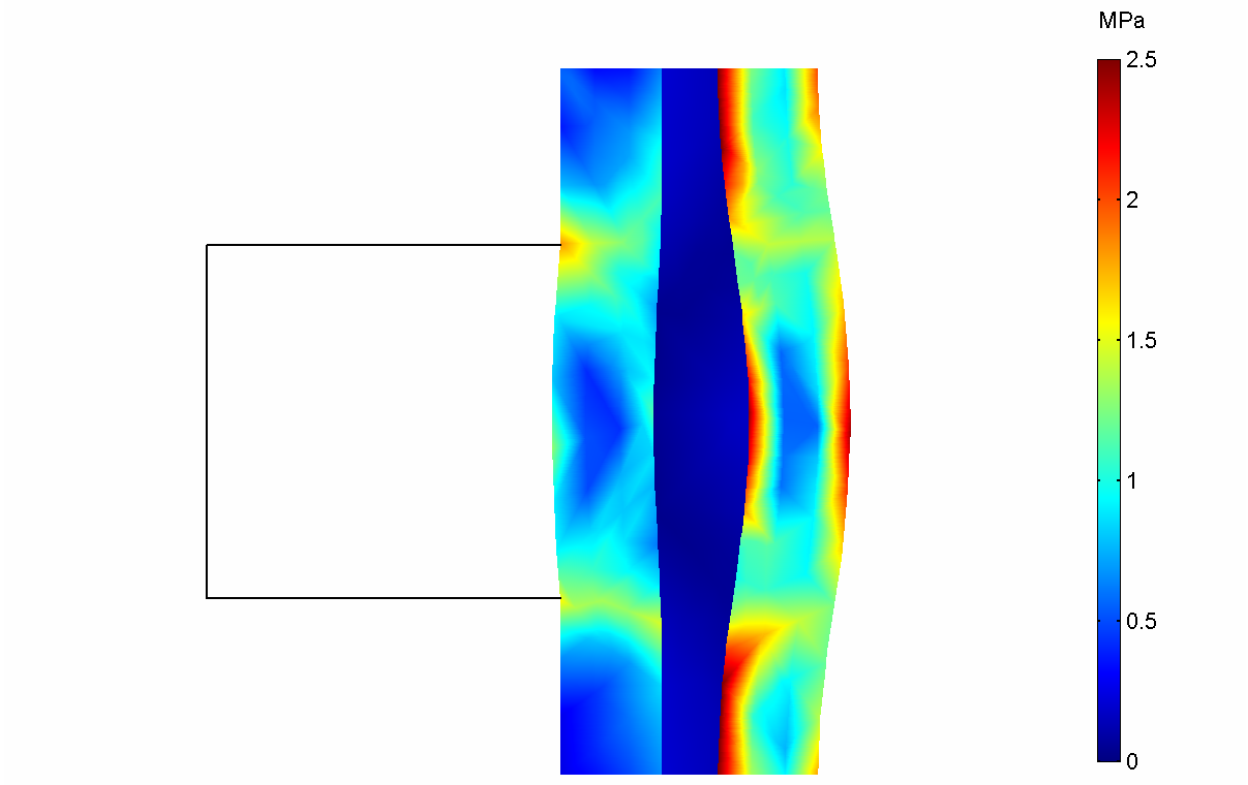

Figure 6. von Mises stress distribution (contour) and deformed shape plot (scale enlarged 200 times) in the MEA at ambient temperature of 300.15 K (27 C) and relative humidity of 80%.

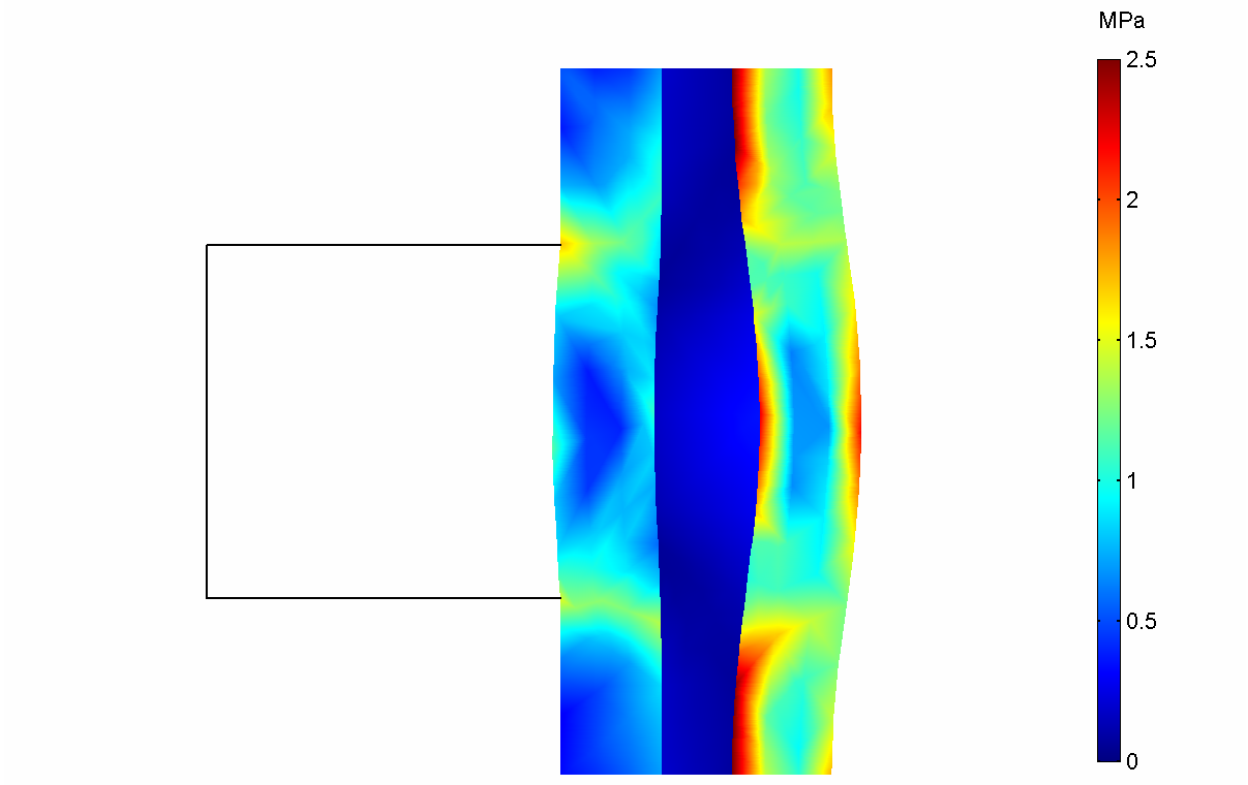

Figure 7. von Mises stress distribution (contour) and deformed shape plot (scale enlarged 200 times) in the MEA at ambient temperature of 300.15 K (27 C) and relative humidity of 20%.

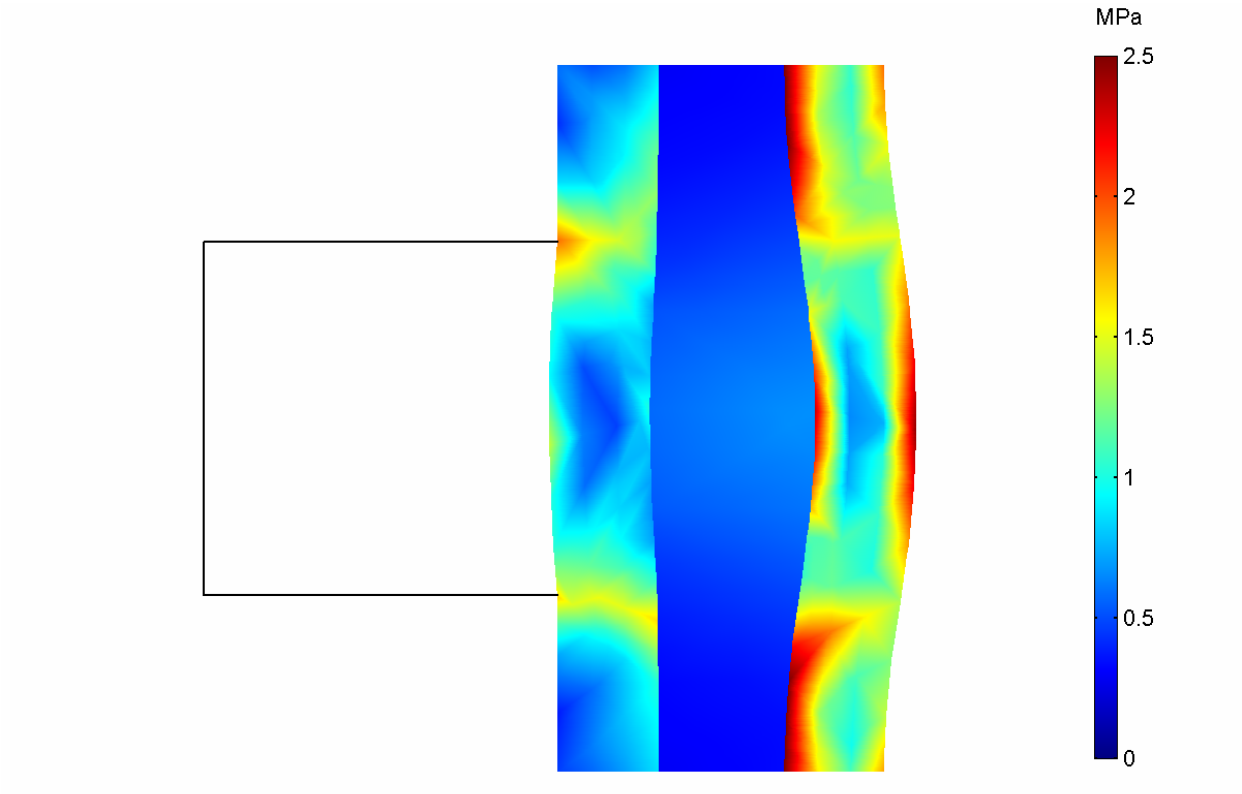

Figure 8. von Mises stress distribution (contour) and deformed shape plot (scale enlarged 200 times) in the MEA at ambient temperature of 318.15 K (45 C) and relative humidity of 80%.

The results show that the non-uniform distribution of stresses, caused by the temperature gradient and moisture change in the cell, induces localized bending stresses, which can contribute to delaminating between the membrane and the gas diffusion layers. The non-uniform distribution of stresses can also contribute to delaminating between the gas diffusion layers and the current collectors. These stresses may explain the occurrence of cracks and pinholes in the fuel cells components under steady–state loading during regular cell operation, especially in the high loading conditions. The results also showed that the ambient conditions (ambient temperature and relative humidity) have a strong impact on the temperature distribution and hygro-thermal stresses inside the cell.

References

[1] Maher A.R. Sadiq Al-Baghdadi. Novel design of a compacted micro-structured air-breathing PEM fuel cell as a power source for mobile phones. International Journal of Energy and Environment IJEE, 2010; 1(4), 555-572.

[2] F. Brèque, J. Ramousse, Y. Dubé, K. Agbossou, P. Adzakpa. Sensibility study of flooding and drying issues to the operating conditions in PEM Fuel Cells. International Journal of Energy and Environment IJEE, 2010; 1(1), 1-20.

[3] Maher A.R. Sadiq Al-Baghdadi. A CFD study of hygro-thermal stresses distribution in tubular-shaped ambient air-breathing PEM micro fuel cell during regular cell operation. International Journal of Energy and Environment IJEE, 2010; 1(2), 183-198.

[4] Maher A.R. Sadiq Al-Baghdadi. Modeling optimizes PEM fuel cell durability using three-dimensional multi-phase computational fluid dynamics model. International Journal of Energy and Environment IJEE, 2010; 1(3), 375-398.

[5] Maher A.R. Sadiq Al-Baghdadi. Mechanical behaviour of PEM fuel cell catalyst layers during regular cell operation. International Journal of Energy and Environment IJEE, 2010; 1(6), 927-936.

[6] Gode, P., Ihonen, J., Strandroth, A., Ericson, H., Lindbergh, G., Paronen, M., Sundholm, F., Sundholm, G., Walsby, N. Membrane Durability in a PEM Fuel Cell Studied Using PVDF Based Radiation Grafted Membranes Fuel Cells. Fuel Cells 2003; 3(1-2), 21-27.

[7] Xie, J., Wood, D.L., Wayne, D.M., Zawodzinski, T., Borup, R.L. Durability of Polymer Electrolyte Fuel Cells at High Humidity Conditions. J. Electrochem. Soc. 2005; 152(1), A104-A113.
[8] Stanic, V., Hoberech, M. Mechanical of pin-hole formation in membrane electrode assemblies for PEM fuel cells. Proceedings of the Fourth International Symposium on Proton Conducting Membrane Fuel Cells, Coral 5, Level 6, Mid Pacific Conference Centre; 2004.
[9] Tang, Y, Karlsson, A.M., Santare, M.H., Gilbert, M., Cleghorn, S., Johnson, W.B. An experimental investigation of humidity and temperature effects on the mechanical properties of perfluorosulfonic acid membrane. J. Materials Science and Engineering 2006; 425(1-2): 297-304.
[10] Webber, A., Newman, J. A Theoretical Study of Membrane Constraint in Polymer-Electrolyte Fuel Cell. AIChE J. 2004; 50(12), 3215–3226.
[11] Tang, Y., Santare, M.H., Karlsson, A.M., Cleghorn, S., Johnson, W.B. Stresses in Proton Exchange Membranes Due to Hygro-Thermal Loading, J.FuelCell Sci.&Tech. ASME 2006; 3(5), 119-124.
[12] Kusoglu, A., Karlsson, A., Santare, M., Cleghorn, S., Johnson, W. Mechanical response of fuel cell membranes subjected to a hygro-thermal cycle. J. Power Sources 2006; 161(2), 987-996.
[13] Fuller E.N., Schettler P.D., Giddings J.C. A new method for prediction of binary gas-phase diffusion coefficients. Ind. Eng. Chem. 1966; 58(5), 18-27.
[14] Berning T., Djilali N. Three-dimensional computational analysis of transport phenomenon in a PEM fuel cell-a parametric study. J. Power Sources 2003; 124(2), 440-452.
[15] Berning T., Djilali N. A 3D, multi-phase, multicomponent model of the cathode and anode of a PEM fuel cell. J. Electrochem. Soc. 2003; 150(12), A1589-A1598.
[16] Nguyen P.T., Berning T., Djilali N. Computational model of a PEM fuel cell with serpentine gas flow channels. J. Power Sources 2004; 130(1-2), 149-157.
[17] Berning T., Lu D.M., Djilali N. Three-dimensional computational analysis of transport phenomena in a PEM fuel cell. J. Power Sources 2002; 106(1-2), 284-294.
[18] Bernadi D.M., Verbrugge M.W. A mathematical model of the solid-polymer-electrolyte fuel cell. J. Electrochem. Soc. 1992; 139(9), 2477-2491.
[19] Gurau V., Liu H., Kakac S. Two-dimensional model for proton exchange membrane fuel cells. AIChE Journal 1998; 44(11), 2410–2422.
[20] Lampinen M.J., Fomino M. Analysis of free energy and entropy changes for half-cell reactions. J. Electrochem. Soc. 1993; 140(12), 3537–3546.
[21] Wang L., Husar A., Zhou T., Liu H. A parametric study of PEM fuel cell performances. Int. J. Hydrogen Energy 2003; 28(11), 1263– 1272.
[22] Parthasarathy A., Srinivasan S., Appleby J.A., Martin C.R. Pressure dependence of the oxygen reduction reaction at the platinum microelectrode/nafion interface: electrode kinetics and mass transport. J.Electrochem.Soc. 1992; 139(10), 2856–2862.
[23] Springer T.E., Zawodzinski T.A., Gottesfeld, S. Polymer electrolyte fuel cell model. J. Electrochem. Soc. 1991; 138(8), 2334-2342.
[24] Siegel N.P., Ellis M.W., Nelson D.J., von Spakovsky M.R. A two-dimensional computational model of a PEMFC with liquid water transport. J. Power Sources 2004; 128(2), 173–184.
[25] Hu M., Gu A., Wang M., Zhu X., Yu L. Three dimensional, two phase flow mathematical model for PEM fuel cell. Part I. Model development. Energy Conversion Manage 2004; 45(11),1861–1882.
[26] Hu M., Gu A., Wang M., Zhu X., Yu L. Three dimensional, two phase flow mathematical model for PEM fuel cell. Part II. Analysis and discussion of the internal transport mechanisms. Energy Conversion Manage 2004; 45(11-12), 1883–1916.
[27] Sivertsen B.R., Djilali N. CFD based modelling of proton exchange membrane fuel cells. J. Power Sources 2005; 141(1), 65-78.
[28] Product Information DuPont™ Nafion® PFSA Membranes N-112, NE-1135, N-115, N-117, NE-1110 Perfluorosulfonic Acid Polymer. NAE101; 2005.

